MOTION ESTIMATION OF AUTONOMOUS SPACECRAFT NEAR ASTEROID USING WIDE-FIELD-INTEGRATION OF OPTIC FLOW

Naoto Kobayashi[(1)], Masataka Oishi[(1)], Yutaka Kinjo[(1)], Daisuke Kubo[(2)], and Shinji Hokamoto[(1)]

[(1)]*Kyushu University, 744 Motooka Nishi-ku Fukuoka 819-0395 Japan, +81-92-802-3039, k-naoto@aero.kyushu-u.ac.jp*

[(2)]*JAXA, 6-13-1 Osawa Mitaka-shi Tokyo 181-0015 Japan*

Abstract: *In this study, a bio-inspired guidance and navigation system is discussed for applying to a deep space probe. Wide-Field-Integration (WFI) of optic flow is a state estimation technique mimicking a visual processing system of some flying insects: e.g., bees, flies, and dragon flies. Optic flow is the vector field of relative velocities obtained by photoreceptors. It is produced from the motion of a projected image over the surface of retina, and WFI of optic flow utilizes a wide range of optic flow for motion estimation. This method is useful as an autonomous guidance and navigation system for spacecrafts, because of its attractive features: applicableness to a low-resolution image sensor, small computational load, and robustness for unknown environment. However, the image region of a camera is limited in a real system unlike the theory of WFI of optic flow. In this paper, how to set up the system is addressed in two conditions: with and without gyro sensors. The effects on the estimation accuracy of optical axes are examined by using numerical simulations and experiments. The results indicate that the adequate elevation directions of optical axes are contrary according to whether gyro sensors are used conjointly or not for its motion estimation. Furthermore, the derived simulation results are verified in some experiments.*

Keywords: *State Estimation, Optic Flow, Wide-Field-Integration.*

1. Introduction

For deep space exploration missions, autonomy is a key technology. Although remote control from Earth is acceptable for a near space mission like activities on Moon, autonomous technologies are indispensable for deep space exploration missions like activities on asteroids. This is because the delay time of signals becomes extremely long in deep space missions. Especially for near-ground maneuvers, such as hover, approach, and landing phases, an autonomous control system is essential since quick response is required for safety[1, 2].

In this study, a bio-inspired guidance and navigation system is investigated for application to a deep space probe. Wide-Field-Integration (WFI) of optic flow is a relative motion estimation technique mimicking a visual processing system of some flying insects: e.g., bees, flies, and dragon flies[3]. Optic flow is produced from the motion of a projected image over the surface of retina[4, 5], and WFI of optic flow utilizes a wide range of optic flow for motion estimation[6, 7, 8, 9, 10]. This method is useful as an autonomous guidance and navigation system for spacecrafts, because of its attractive features. First, the system can be composed of a small, light-weight, low-resolution image sensor, because the accuracy of each optic flow is less important in the integration process. Thus such a hardware device can be mounted for spacecraft under a severe weight constraint. Second, the computational load is small and thus quick response is possible, because the estimation

process is relatively simple. And finally, the estimation results are robust for asteroid surfaces due to the integration process for many optic flow. Consequently, it is effective even for uncertain environments. From these attractive features, this method is expected as an autonomous navigation system of spacecrafts. Furthermore, the WFI of optic flow sensor can be used as a back-up system for the malfunction of gyro sensors, although spacecraft equips with gyro sensors for its attitude control.

However, there are few researches about applying WFI of optic flow to a guidance and navigation system of three-dimensional flying object. The main reason comes from the gap between the theoretical assumptions and the restrictions of practical systems in the estimation process. The theory of WFI of optic flow assumes that the optic flow is obtained in the whole area of a spherical image surface around the vehicle's mass center. However in a real system, optic flow is obtained from an image sensor with a limited field of view. Even with multiple cameras, it is not realistic to obtain optic flow in the whole area of a spherical image surface. Furthermore, the image surface of a standard camera is not spherical but flat, and sensor outputs of real systems include noises.

In this paper, how to set up the system is addressed from the evaluation of the estimation accuracy by numerical simulations and experiments. Especially, the elevation direction of optical axes are examined, since the effect on azimuth directions has discussed in our previous study. Considering the possibility of a WFI of optic flow sensor as a back-up system for gyro sensors, we examine two cases. In the former case, the angular velocities are obtained from gyro sensors and only translational velocities are estimated from the WFI of optic flow system, while the latter estimates both translational and rotational velocities simultaneously. The results indicates opposite tendency for adequate elevation direction of optical axes whether gyro sensors are used conjointly or not, and suggest that how image sensors should be arranged according to mission scenarios and other sensors.

The paper is organized as follows. The basics of WFI of optic flow theory are described in Sec. 2. The effects on the estimation accuracy of the directions of image sensors are investigated with numerical simulations in Sec. 3. In Sec. 4, the results of the numerical simulations are verified using actual hardware devices mounted on a multirotor vehicle, which is an experimental model of spacecrafts flying near an asteroid surface. Sec. 5 concludes the paper.

2. Description of Wide-Field-Integration of Optic flow

2.1. Optic flow model

Fig. 1 shows a spacecraft flying near the surface of an asteroid. (x_b, y_b, z_b) is a vehicle fixed coordinate system whose origin is attached to its mass center. In the WFI method, optic flow is assumed to be obtained from each photoreceptor on a spherical image surface, which is set around the vehicle's mass center. The position of each photoreceptor on the sphere is described with the azimuth γ and elevation β angles. The angle γ is measured positive from the x_b axis, and the angle β is measured positive from the z_b axis. Then, the line-of-sight vector $\boldsymbol{Q}$ for a fiducial point on the

asteroid surface is written with β and γ angles as follows:

$$\boldsymbol{Q} = \begin{bmatrix} \sin\beta\cos\gamma & \sin\beta\sin\gamma & \cos\beta \end{bmatrix}^T \tag{1}$$

Fiducial points on the surface are assumed stationary relative to the reference frame (x_t, y_t, z_t) fixed on the environmental terrain. The time derivative of $\boldsymbol{Q}$ indicates the motion parallax $\dot{\boldsymbol{Q}}$, which is caused by the motion of translational and angular velocities of the probe. Let $\boldsymbol{v} = [u\ v\ w]^T$ be the translational velocity and $\boldsymbol{\omega} = [p\ q\ r]^T$ be the angular velocity, then optic flow can be written as follows:

$$\dot{\boldsymbol{Q}} = -\boldsymbol{\omega} \times \boldsymbol{Q} - \mu\left(\boldsymbol{v} - \langle \boldsymbol{v}, \boldsymbol{Q} \rangle \boldsymbol{Q}\right) \tag{2}$$

where $\langle *, * \rangle$ denotes the inner product, and the nearness function μ is the inverse of the distance to the fiducial points on the terrain. The optic flow is divided to γ and β components like $\dot{\boldsymbol{Q}} = \dot{Q}^{\gamma}\boldsymbol{e}_{\gamma} + \dot{Q}^{\beta}\boldsymbol{e}_{\beta}$, and they are written as follows:

$$\dot{Q}^{\gamma} = p\cos\beta\cos\gamma + q\cos\beta\sin\gamma - r\sin\beta + \mu\left(u\sin\gamma - v\cos\gamma\right) \tag{3}$$

$$\dot{Q}^{\beta} = p\sin\gamma - q\cos\gamma - \mu\left(u\cos\beta\cos\gamma + v\cos\beta\sin\gamma - w\sin\beta\right) \tag{4}$$

Assuming that surrounding environment is a flat, infinite, and horizontal plane, the nearness function μ is expressed with attitude angles (ϕ, θ):

$$\mu = \frac{-\sin\beta\cos\sin\gamma\sin\theta + \sin\beta\sin\gamma\sin\phi\cos\sin\theta + \cos\sin\beta\cos\sin\phi\cos\sin\theta}{z} \tag{5}$$

Note that for uneven terrain surfaces, the WFI of optic flow method virtually assumes a flat surface and estimates the motion of the probe relative to the virtual surface.

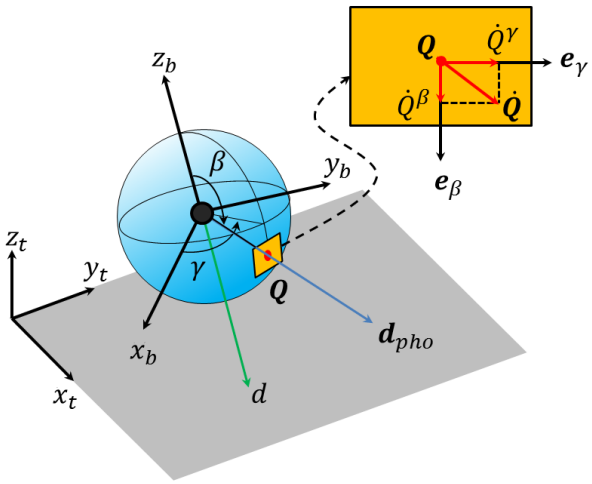

Figure 1. Model of Wide-Field-Integration of optic flow

2.2. Wide-Field-Integration

A sensitivity function is expressed as $\boldsymbol{F_j} = F_j^{\gamma}\boldsymbol{e}_{\gamma} + F_j^{\beta}\boldsymbol{e}_{\beta}$, and the jth WFI output is defined with a jth sensitivity function as follows:

$$y_j = \int \dot{\boldsymbol{Q}} \cdot \boldsymbol{F_j}\, d\Omega = \int \left(\dot{Q}^{\gamma}F_j^{\gamma} + \dot{Q}^{\beta}F_j^{\beta}\right) d\Omega \tag{6}$$

where $d\Omega = \sin\beta\, d\beta\, d\gamma$ is a solid angle on the sphere. Spherical harmonics is used as a sensitivity function in this paper. When M is used for the number of the spherical harmonics modes, $M \times 1$ measurement vector of WFI outputs can be constructed as $\boldsymbol{y} = [y_1 \ \cdots \ y_M]^T$.

$$\boldsymbol{y} = \left[\ \int \left(\dot{Q}^{\gamma} F_1^{\gamma} + \dot{Q}^{\beta} F_1^{\beta} \right) d\Omega \quad \cdots \quad \int \left(\dot{Q}^{\gamma} F_M^{\gamma} + \dot{Q}^{\beta} F_M^{\beta} \right) d\Omega \ \right]^T \tag{7}$$

Although Eq. 7 is a standard expression of WFI output introduced in [11], in this paper, the following equations are adopted as the equations of WFI output.

$$\boldsymbol{y} = \left[\ (\boldsymbol{y}^{\gamma})^T \quad \left(\boldsymbol{y}^{\beta}\right)^T \ \right]^T \tag{8}$$

$$\boldsymbol{y}^{\gamma} = \left[\ \int \dot{Q}^{\gamma} F_1^{\gamma} \, d\Omega \quad \cdots \quad \int \dot{Q}^{\gamma} F_M^{\gamma} \, d\Omega \ \right]^T \tag{9}$$

$$\boldsymbol{y}^{\beta} = \left[\ \int \dot{Q}^{\beta} F_1^{\beta} \, d\Omega \quad \cdots \quad \int \dot{Q}^{\beta} F_M^{\beta} \, d\Omega \ \right]^T \tag{10}$$

where WFI output $\boldsymbol{y} = \left[y_1^{\gamma} \ \cdots \ y_M^{\gamma} \, y_1^{\beta} \ \cdots \ y_M^{\beta} \right]^T$ becomes $2M \times 1$ measurement vector.

Ideally, the optic flow $\dot{\boldsymbol{Q}}$ is regarded as a continuous function, and WFI output is calculated from the integration of the inner product between the optic flow $\dot{\boldsymbol{Q}}$ and the sensitivity function $\boldsymbol{F}$. However, in a realistic system, the optic flow data is obtained at discretized points on an image sensor. Paper [12] revealed that the evaluation of WFI of optic flow is still reliable for discrete data accompanied by Riemann sums. Approximating the integration by Riemann sums, the actual WFI output is obtained as follows:

$$\boldsymbol{y} = \begin{bmatrix} \displaystyle\sum_{k=1}^{N} \dot{Q}^{\gamma}(\gamma_k, \beta_k, \boldsymbol{x}) F_1^{\gamma}(\gamma_k, \beta_k) \Delta\Omega \\ \vdots \\ \displaystyle\sum_{k=1}^{N} \dot{Q}^{\gamma}(\gamma_k, \beta_k, \boldsymbol{x}) F_M^{\gamma}(\gamma_k, \beta_k) \Delta\Omega \\ \displaystyle\sum_{k=1}^{N} \dot{Q}^{\beta}(\gamma_k, \beta_k, \boldsymbol{x}) F_1^{\beta}(\gamma_k, \beta_k) \Delta\Omega \\ \vdots \\ \displaystyle\sum_{k=1}^{N} \dot{Q}^{\beta}(\gamma_k, \beta_k, \boldsymbol{x}) F_M^{\beta}(\gamma_k, \beta_k) \Delta\Omega \end{bmatrix} \tag{11}$$

where N is the total number of optic flow data. This WFI output $\boldsymbol{y}$ is a nonlinear function, and it can be expressed as $\boldsymbol{y} = g(\boldsymbol{X})$ for a state vector $\boldsymbol{X}$.

The state vector $\boldsymbol{X}$ is composed of all state variables: $\boldsymbol{X} = [u \ v \ w \ p \ q \ r \ \phi \ \theta \ z]^T$. However since a flat surface is assumed, the position x,y and yaw angle ψ are not included. Furthermore, the altitude z and the roll and pitch attitude angles ϕ, θ are assumed to be obtained from other sensors in this paper, thus only the translational and angular velocities are estimated using WFI of optic flow. Thus, after linearization, $\boldsymbol{y}$ can be expressed for the state vector $\boldsymbol{x} = [u \ v \ w \ p \ q \ r]^T$ as follows:

$$\boldsymbol{y} = \boldsymbol{C}(\phi, \theta, z)\, \boldsymbol{x} \tag{12}$$

Table 1. Typical surveillance flight condition of a space probe used in simulations

(ϕ, θ, ψ) [deg]	$(0,0,0)$
z [m]	200
(u,v,w) [m/s]	$(10.0, 10.0, 0)$
(p,q,r) [deg/s]	$(0,0,0)$

Table 2. Directions of optical axes used in simulations

		(β_1, β_2) [deg]	(γ_1, γ_2) [deg]
Case 1 or 2	a	(150, 150)	(0, 90)
	b	(135, 135)	(0, 90)
	c	(120, 120)	(0, 90)

where $\boldsymbol{C}$ is an observation matrix of $2M \times 6$ including (ϕ, θ, z) parameters. Then, the state parameters are estimated through the pseudo inverse matrix $\boldsymbol{C}^{\dagger}$.

$$\boldsymbol{x} = \boldsymbol{C}^{\dagger}(\phi, \theta, z)\, \boldsymbol{y} \tag{13}$$

When the attitude angular rates p, q and r can be obtained by onboard gyro sensors, the state variables $\boldsymbol{x}$ is replaced by $\boldsymbol{x_s} = [u\ v\ w]^T$. Then the state is estimated as follows:

$$\boldsymbol{x_s} = \boldsymbol{C}^{\dagger}(\phi, \theta, z, p, q, r)\, \boldsymbol{y} \tag{14}$$

3. Numerical simulation

As mentioned above, optic flow is assumed in theory to be obtained from a whole spherical image surface around the mass center of the vehicle. On the other hand, in a real system, optic flow is obtained from a image sensor with a limited field of view. In this section, the effects on estimation accuracy of elevation directions of optical axes are investigated in numerical simulations considering sensor noises. The effects are examined in two cases, with and without gyro sensors; in the former case only translational velocities are estimated, while the latter both translational and rotational velocities are estimated simultaneously.

One of surveillance flight conditions of a space probe shown in Tab. 1 is used in simulations. The field of view of a camera used in simulations is defined as 30 and 40 degrees in its elevation and azimuth directions, respectively, referred to a real optic flow sensor. Since preliminary studies (the results have been submitted to a journal and now under reviewing) have revealed that one optic flow sensor easily misestimates the vehicle's motion, two optic flow sensors are considered in numerical simulations to secure estimation accuracy. The directions of cameras are listed in Tab. 2. Subscripts of 1 and 2 in the table indicates cameras number. As can be seen elevation directions of optical axes of the cameras are changed, and its effect is investigated. Sensor noises included in the optic flow is assumed to be white noises, whose mean value is zero and standard deviation is 0.3. Moreover, noises of gyro sensors are also assumed to be white noises, whose mean value is zero and standard deviation is 0.05. In Case 1, the system is assumed to have gyro sensors, and only the translational velocities of a space probe are estimated from Eq. 14. While in Case 2, the translational and rotational states of the space probe are estimated from Eq. 13. The results are compared in the mean values and standard deviations of the estimation errors on each case.

Table 3. Mean values of estimation error in Case 1

	u	*v*	*w*
Case 1a	10.23	9.01	5.33
Case 1b	12.38	10.55	7.00
Case 1c	16.47	15.77	11.04

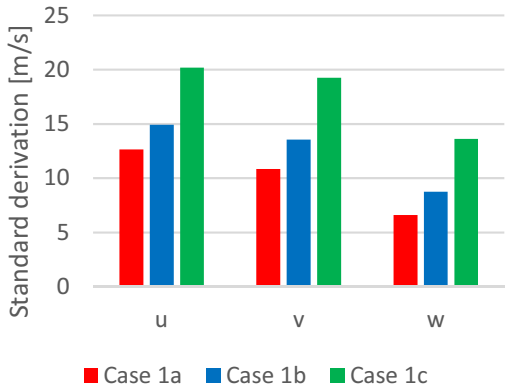

Figure 2. Standard deviations of estimation error in Case 1

Tab. 3 and Fig. 2 shows the mean values and the standard deviations of the obtained estimation errors in Case 1. These results indicate that the estimation accuracy of all translational velocities become worse as the elevation direction of the optical axis changes from 150 to 120 degrees. This implies that image sensors should be faced near the bottom of the vehicle.

Table 4. Mean values of estimation error in Case 2

	u	*v*	*w*	*p*	*q*	*r*
Case 2a	12.55	11.10	7.91	2.96	3.40	1.17
Case 2b	7.40	6.97	6.00	1.64	1.73	0.75
Case 2c	6.08	7.04	5.86	1.12	1.07	0.72

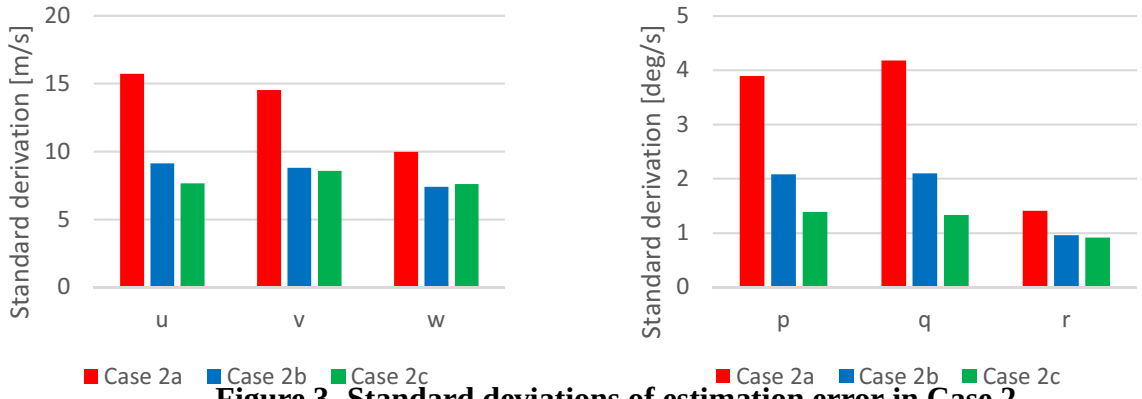

Figure 3. Standard deviations of estimation error in Case 2

On the other hand, Tab. 4 and Fig. 3 show the mean values and the standard deviations of the obtained estimation errors in Case 2. These results indicate that the estimation accuracy of all state

Table 5. Specifications of the optic flow sensor

Resolution (H)×(V) [px]	320×240
Number of optic flow data (H)×(V) [-]	79×59
Field of view (H)×(V) [deg]	45.1×34.6
Frame rate [fps]	0.1

parameters become better as the elevation direction of the optical axis changes from 150 to 120 degrees. This implies that the directions of image sensors should be faced to near a horizontal direction. However, note that optic flow cannot be obtained in a hemisphere upper than horizontal revel. Thus, the elevation direction of optic flow sensors should be decided considering the field of view of image sensors and the expected attitude change.

It should be emphasized that from the comparison between Case 1 and Case 2, the adequate direction of optic flow sensors are contrary according to whether the probe utilizes gyro sensors or not for its motion estimation. This implies that mounting angles of image sensors should be arranged according to the mission to apply WFI of optic flow to a real system.

4. Preliminary experiments using a real optic flow sensor

In this section, the effects on the estimation accuracy of the elevation directions of optical axes is investigated with experiments using a real sensor system to verify the results obtained in the numerical simulations. The specifications of an image sensor used in the experiments are shown in Tab. 5. Optic flow can be obtained at points (79×59) in the field of view $(45.1\,\mathrm{deg} \times 34.6\,\mathrm{deg})$ at every 0.1 second. Two image sensors have been mounted on a multirotor, which is an experimental system modeling a spacecraft flying near an asteroid surface. In the experiments, the state variables of the vehicle are measured by a motion capture apparatus, for the comparison with the estimation results obtained from the WFI of optic flow system. Directions of optical axis used in the experiments are same as shown in Tab. 2. However in this experiment, since gyro sensors are not mounted on the vehicle, six motion velocities are estimated from the optic flow sensor and the motion capture system. The estimation results are denoted as Case 3.

Fig. 4 shows, as an example, the time histories of the estimation results in Case 3b. Red lines are the estimation results from WFI of optic flow, and black lines are the motion variables measured by the motion capture apparatus. Note that the variables obtained by the motion capture also include errors due to noises and discretization, thus they are not "true". Tab. 6 and Fig. 5 show the mean values and the standard deviations of estimation error in three cases. These results show that the estimation accuracy of almost all the state variables becomes better according to the directions of optical axes approach to a horizontal direction; this is consistent with the result in the numerical simulations.

Table 6. Mean values of estimation error in Case 3

	u	*v*	*w*	*p*	*q*	*r*
Case 3a	0.10	0.14	0.11	11.54	12.33	5.91
Case 3b	0.05	0.06	0.07	4.92	4.71	5.55
Case 3c	0.06	0.08	0.06	4.58	3.59	5.27

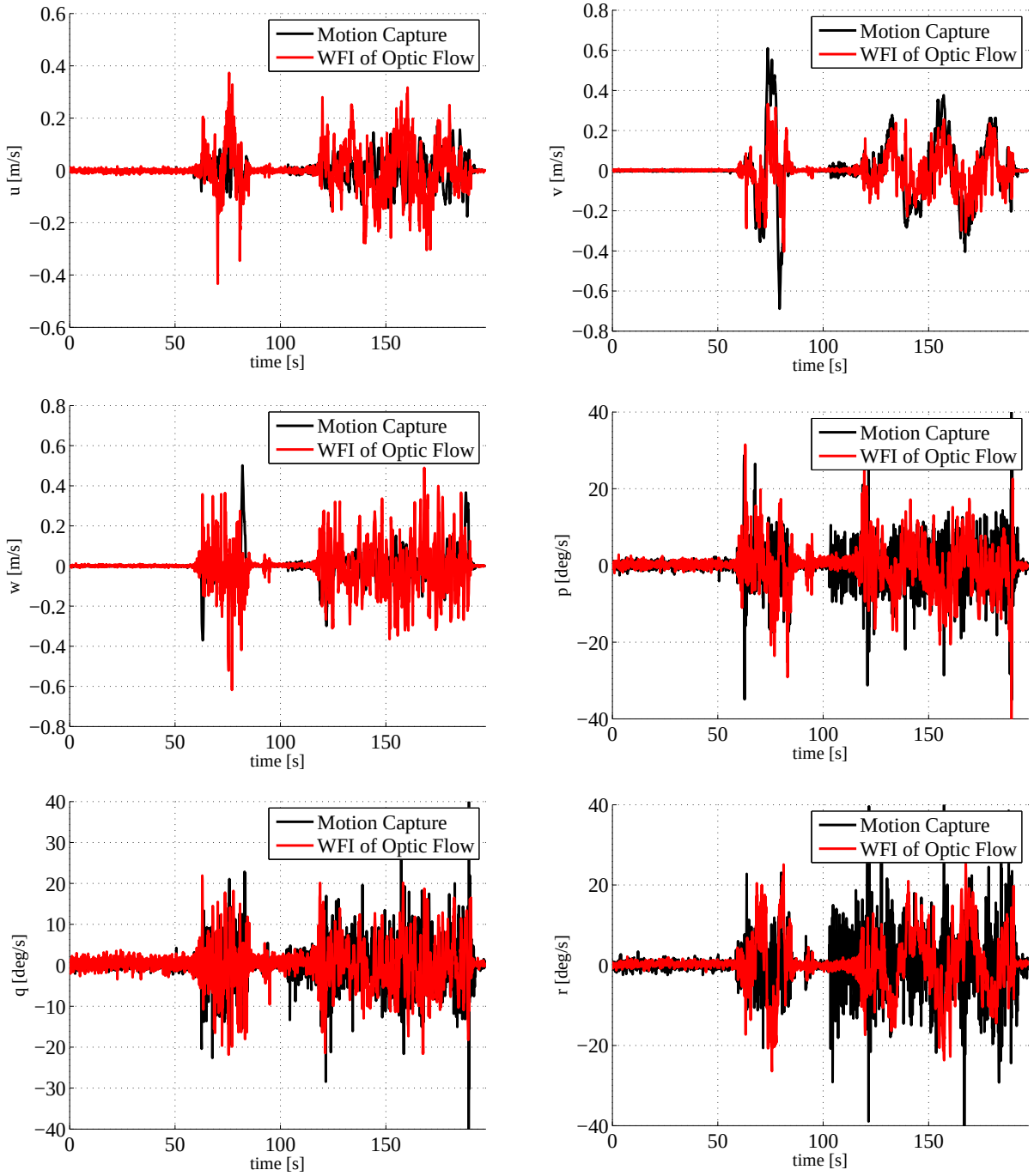

Figure 4. Time histories of the estimation results in Case 3b

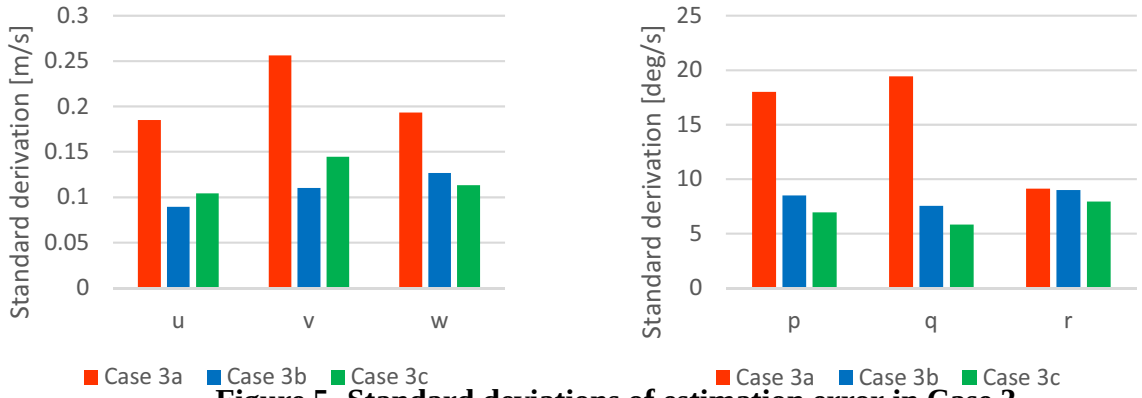

Figure 5. Standard deviations of estimation error in Case 3

5. Conclusion

This paper discussed how to apply WFI of optic flow sensors to a guidance and navigation system for spacecrafts flying near asteroid surface, considering the restrictions of practical hardware systems. Since in our previous studies revealed that more than two cameras should be mounted for obtaining better estimation accuracy and discussed the effects of the azimuth direction of optical axes, in this paper the effects on estimation accuracy of the elevation directions of optical axes were examined. Moreover, two cases have been mainly considered: one has gyro sensors and only translational velocities are estimated for the WFI of optic flow system, and another estimates six parameters (: translational and rotational velocities). The results of the numerical simulations indicated that the proper directions of the optical axes are contrary according to whether the spacecraft utilizes gyro sensors or not. Furthermore, the obtained simulation results were verified with some preliminary experiments.

6. References

[1] Thakoor, S., Morookian, J., Chahl, J., Hine, B., and Zornetzer, S. "BEES: Exploring Mars with Bioinspired Technologies." Computer, Vol. 37, No. 9, pp. 38–47, 2004.

[2] Izzo, D., Weiss, N., and Seidl, T. "Constant-Optic-Flow Lunar Landing: Optimality and Guidance." Journal of Guidance, Control, and Dynamics, Vol. 34, No. 5, pp. 1383–1395, 2011.

[3] Egelhaaf, M., Kern, R., Krapp, H. G., Kretzberg, J., Kurtz, R., and Warzecha, A. "Neural encoding of behaviourally relevant visual-motion information in the fly." Trends in Neurosciences, Vol. 25, pp. 96–102, 2002.

[4] Gibson, J. The Perception of the Visual World. Houghton Mifflin, 1950.

[5] Koenderink, J. J. and van Doorn, A. J. "Facts on Optic Flow." Biological Cybernetics, Vol. 56, No. 4, pp. 247–254, 1987.

[6] Humbert, J. S. Bio-Inspired Visuomotor Convergence in Navigation and Flight Control Systems. Ph.D. thesis, Mechanical Engineering Department, California Inst. of Technology, Pasadena, CA, 2005.

[7] Conroy, J., Gremillion, G., Ranganathan, B., and Humbert, J. S. "Implementation of Wide-Field Integration of Optic Flow for Autonomous Quadrotor Navigation." Autonomous Robots, Vol. 27, No. 3, pp. 189–198, 2009.

[8] Humbert, J. S. and Hyslop, A. M. "Bio-Inspired Visuomotor Convergence." IEEE Transactions on Robotics, Vol. 26, No. 1, pp. 121–130, 2010.

[9] Hyslop, A. M., Krapp, H. G., and Humbert, J. S. "Control Theoretic Interpretation of Directional Motion Preferences in Optic Flow Processing Interneurons." Biological Cybernetics, Vol. 103, No. 5, pp. 353–364, 2010.

[10] Humbert, J. S., Murray, R. M., and Dickinson, M. H. "Pitch-Altitude Control and Terrain Following Based on Bio-Inspired Visuomotor Convergence." "Correction of Technical Papars - AIAA Guidance, Navigation, and Control Conference," Vol. 6, pp. 4407–4418. August 2005.

[11] Hyslop, A. M. and Humbert, J. S. "Autonomous Navigation in Three-Dimensional Urban Environments Using Wide-Field Integration of Optic Flow." Journal of Guidance, Control, and Dynamics, Vol. 33, No. 1, pp. 147–159, 2010.

[12] Shoemaker, M. A. and Hokamoto, S. "Comparison of Integrated and Nonintegrated Wide-Field Optic Flow for Vehicle Navigation." Journal of Guidance, Control, and Dynamics, Vol. 36, No. 3, pp. 710–720, 2013.